SAE INTERNATIONAL

AUTOMOTIVE

Progress in Modeling and Simulation of Batteries

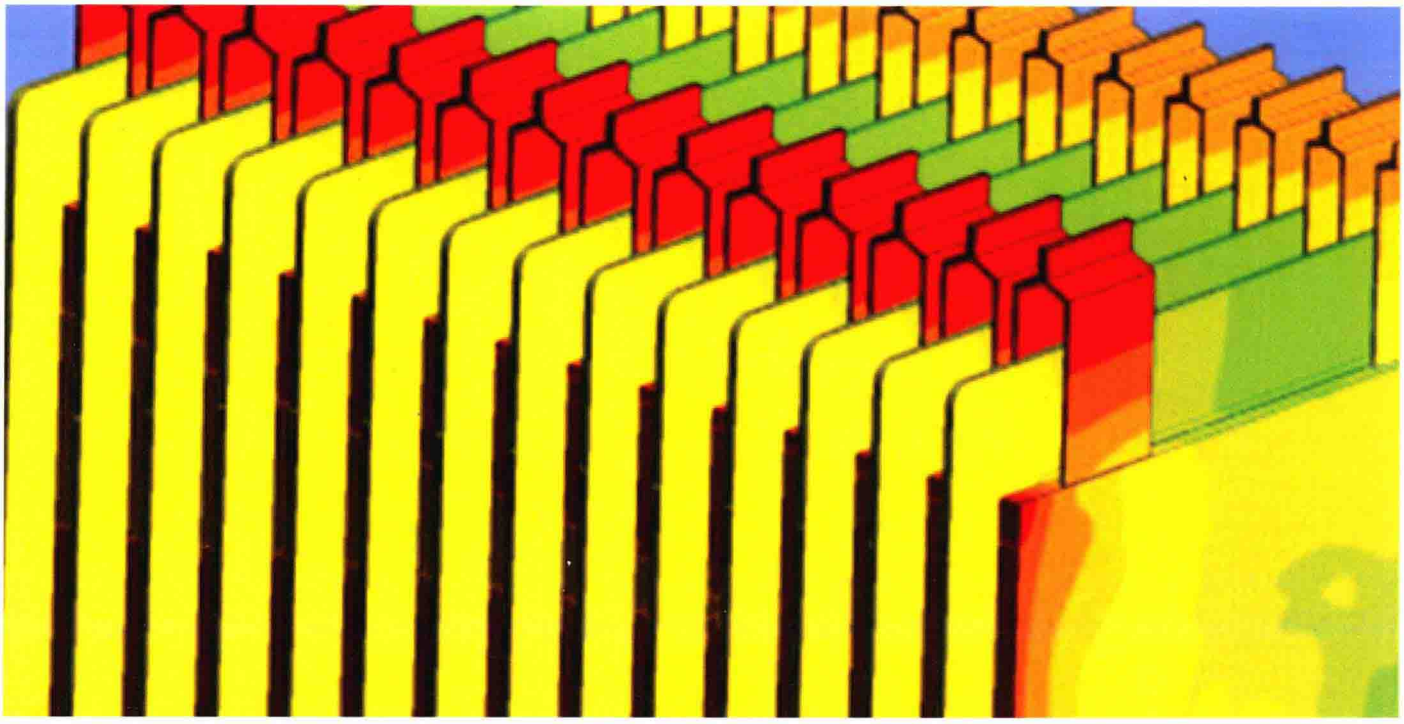

Edited by:
John A. Turner

Progress in Modeling and Simulation of Batteries

Edited by John A. Turner

SAE INTERNATIONAL

Warrendale, Pennsylvania, USA

400 Commonwealth Drive
Warrendale, PA 15096-0001 USA
E-mail: CustomerService@sae.org
Phone: +1.877.606.7323 (inside USA and Canada)
+1.724.776.4970 (outside USA)
Fax: +1.724.776.0790

Library of Congress Catalog Number 2015957339
SAE Order Number PT-176
http://dx.doi.org/10.4271/pt-176

ISBN-Print 978-0-7680-8282-1
ISBN-PDF 978-0-7680-8366-8
ISBN-epub 978-0-7680-8368-2
ISBN-prc 978-0-7680-8367-5

Progress in Modeling and Simulation of Batteries

Other SAE books of interest:

Lithium Ion Batteries in Electric Vehicles
Ahmad Pesaran
(Product Code: PT-175)

Electric and Hybrid Electric Vehicles
Ronald K. Jurgen
(Product Code: PT-143.SET)

Electric and Hybrid Electric Vehicles - Batteries
Ronald K. Jurgen
(Product Code: PT-143/2)

Battery Reference Book
T.R. Compton
(Product Code: R-167)

Future Automotive Fuels and Energy
Bruce Morey
(Product Code: T-128)

For more information or to order a book, contact:

SAE INTERNATIONAL
400 Commonwealth Drive
Warrendale, PA 15096-0001, USA;

Phone: +1.877.606.7323 (U.S. and Canada only)
or +1.724.776.4970 (outside U.S. and Canada)
Fax: +1.724.776.0790
Email: CustomerService@sae.org
Website: books.sae.org

Table of Contents

Introduction 1

1. **Characterizing Thermal Behavior of an Air-Cooled Lithium-Ion Battery System for HEV Applications Using FEA Approach (2013-01-1520)** 3
   Kim F. Yeow and Ho Teng, AVL Powertrain Engineering Inc.

2. **AutoLion™: A Thermally Coupled Simulation Tool for Automotive Li-Ion Batteries (2013-01-1522)** 13
   Jim Kalupson, Gang Luo and Christian E. Shaffer, EC Power

3. **Simplified Extended Kalman Filter Observer for SOC Estimation of Commercial Power-Oriented LFP Lithium Battery Cells (2013-01-1544)** 19
   Tarun Huria and Massimo Ceraolo, Università di Pisa
   Javier Gazzarri and Robyn Jackey, MathWorks

4. **A Complete Li-Ion Battery Simulation Model (2014-01-1842)** 29
   Xiao Hu and Scott Stanton, ANSYS Inc.

5. **Comparison of Optimization Techniques for Lithium-Ion Battery Model Parameter Estimation (2014-01-1851)** 37
   Adam Ing, Ramin Masoudi, and John McPhee, University of Waterloo
   Thanh-Son Dao, Maplesoft

6. **Physics-Based Models, Sensitivity Analysis, and Optimization of Automotive Batteries (2014-01-1865)** 47
   Joydeep Banerjee and John McPhee, Univ. of Waterloo
   Paul Goossens and Thanh-Son Dao, Maplesoft

7. **Three-Dimensional Electrochemical Analysis of a Graphite/LiFePO4 Li-Ion Cell to Improve Its Durability (2015-01-1182)** 59
   Mehrdad Mastali Majdabadi Kohneh and Ehsan Samadani, University of Waterloo
   Siamak Farhad, University of Akron

8. **Experimental Measurements of Thermal Characteristics of LiFePO4 Battery (2015-01-1189)** 67
   Satyam Panchal, Scott Mathewson, Roydon Fraser, Richard Culham, and Michael Fowler, University of Waterloo

9. Will Your Battery Survive a World With Fast Chargers? (2015-01-1196) 79
Jeremy S. Neubauer and Eric Wood, National Renewable Energy Laboratory

About the Editor 89

Introduction

Even as the price of transportation fuels fluctuates, interest in hybrid and fully electric powered vehicles continues to grow, driven by environmental, economic, and national security motives. Research and development efforts spanning universities, industry, and research institutions strive for ever higher energy and power densities, lower cost, and improved safety, all of which will further accelerate interest and adoption.

It is also increasingly recognized that modeling and simulation can play a significant role in these efforts, working in conjunction with both theory and experiment, as it has in other fields such as aircraft design, vehicle crash safety, vehicle aerodynamics, and nuclear weapons. Indeed, in some of these fields, particularly where experiments are difficult, expensive, or prohibited, modeling and simulation has become the foundation on which progress is built - at times leading theory and/or experiments.

Although as a community we have not reached that level of predictive capability in modeling and simulation of batteries, significant progress has been made over the last few years. In this volume we present nine examples of this progress. Note that several of the included works focus on thermal behavior, and that we have included one experimental study of thermal characteristics due to its potential use in validating the simulation capabilities. Studies presented here range from fast-running approaches potentially useful in battery management system design and analysis to moderately high-fidelity 3D capabilities, and include the work of universities, industry and research institutions.

This is a fast-moving field, and progress is on-going, with more accurate models and more capable simulation tools under constant development. As a result, this collection represents a snapshot of capability and directions, and we look forward to the next advances in modeling and simulation capability. Some examples include tighter nonlinear coupling of physical phenomena, increased integration of sub-grid micro- and meso-scale simulations, and more integrated sensitivity and uncertainty analysis. In the meantime, we hope that this collection provides useful and compelling evidence of the progress in modeling and simulation of batteries.

John A. Turner
Computational Engineering & Energy Sciences Group Leader
Oak Ridge National Laboratory (ORNL)
Computer Science and Mathematics Division

Chief Computational Scientist
Consortium for Advanced Simulation of Light Water Reactors (CASL)

Joint Faculty Professor, University of Tennessee
Bredesen Center for Interdisciplinary Research and Graduate Education; Knoxville, Tennessee
National Center for Computational Engineering; Chattanooga, Tennessee

SAE International

Characterizing Thermal Behavior of an Air-Cooled Lithium-Ion Battery System for Hybrid Electrical Vehicle Applications Using Finite Element Analysis Approach

2013-01-1520
Published
04/08/2013

Kim F. Yeow and Ho Teng
AVL Powertrain Engineering Inc.

doi:10.4271/2013-01-1520

ABSTRACT

Thermal behavior of a Lithium-ion (Li-ion) battery module under a user-defined cycle corresponding to hybrid electrical vehicle (HEV) applications is analyzed. The module is stacked with 12 high-power 8Ah pouch Li-ion battery cells connected in series electrically. The cells are cooled indirectly with air through aluminum cooling plate sandwiched between each pair of cells. The cooling plate has extended cooling surfaces exposed in the cooling air flow channel. Thermal behavior of the battery system under a user specified electrical-load cycle for the target hybrid vehicle is characterized with the equivalent continuous load profile using a 3D finite element analysis (FEA) model for battery cooling. Analysis results are compared with measurements. Good agreement is observed between the simulated and measured cell temperatures. Improvement of the cooling system design is also studied with assistance of the battery cooling analyses. The results of this study demonstrate that the 3D FEA battery cooling model developed in this study can reasonably characterize thermal behavior of the Li-ion battery systems under the dynamic discharge-charge cycle. The correlated FEA model can be used to evaluate and/or optimize the cooling system designs for the battery systems with indirect air cooling.

INTRODUCTION

The battery packs for HEV applications usually consist of multiple identical battery modules connected in series to achieve the required pack voltage. Within each of the battery modules, the cells are connected in a certain series-parallel configurations to achieve the required capacity and voltage. In an ideal battery pack design, all the modules in the pack would be thermally symmetric, i.e., have identical cooling conditions. As such the cooling system of a battery module is the basic cooling system for a battery pack. The maximum cell temperatures and the maximum differential cell temperatures for the cells in the battery pack are crucial to the performance of the battery system. In operations under cold ambient, the coolest cell within the pack determines the maximum pack power. On the other hand, in operations under elevated ambient temperatures, the hottest cell within the pack limits the maximum allowed current for safe pack utilizations.

The state of charge (SOC) for the HEV battery pack is typically controlled in a SOC range from 0.35 to 0.65 (i.e., $\Delta SOC = 0.3$) with $SOC = 0.5$ being a reference point for the SOC balance. Because of its narrow usable SOC range, a HEV battery pack experiences high discharge/charge pulse currents in pack utilizations. These high-pulse and high-frequency discharge/charge activities generate considerable amount of heat within the battery cells, resulting in high cell temperatures if the cell heat cannot be dissipated into the cooling medium rapidly. The maximum cell temperatures and the maximum differential cell temperatures are crucial factors to the performance, safety and durability of a battery system. Thus, these temperatures must be monitored and controlled by the battery thermal management system. A good battery thermal management system design lies on good understanding of the thermal behavior of the cells in the battery pack. Thermal modeling of the cells and modules can play an important role in understanding the thermal behavior of the battery cells under specified pack duties. This paper discusses the use of 3D FEA model in analyzing the thermal

behavior of a battery system with indirect air cooling under a thermal load condition simulating HEV applications. Improvement of the battery cooling system design with assistance of the battery thermal analysis will also be discussed.

BATTERY SYSTEM DESCRIPTION

The battery pack under study consists of 8 identical modules with each stacked with twelve 8Ah Li-ion pouch cells connected in series, giving a 96S1P pack configuration. Specifications of the cells are given in Table 1. If the pack cooling air flow is assumed to be equally distributed among all modules, i.e., the 8 modules are thermally symmetric, then only a representative module needs to be studied. Figure 1 illustrates the FEA model of the battery module under study. Each pair of cells within the module is cooled via a 2-mm thick aluminum cooling plate sandwiched between them. The aluminum cooling plate has extended surfaces (hereafter refers to as cooling fins) that are in the air flow channel. Such a cooling system may be defined as an indirect air cooling system. The side surface of the cell that is not in contact with the cooling plate is in contact with an elastomeric thermal pad. The module frame is made of plastic, which is not modeled because heat transfer through it is negligible in comparison to that through the cooling fins. The battery cell temperatures can be controlled by the air temperature and/or the heat transfer coefficient (HTC) on the cooling fins by varying the air flow in the cooling channel.

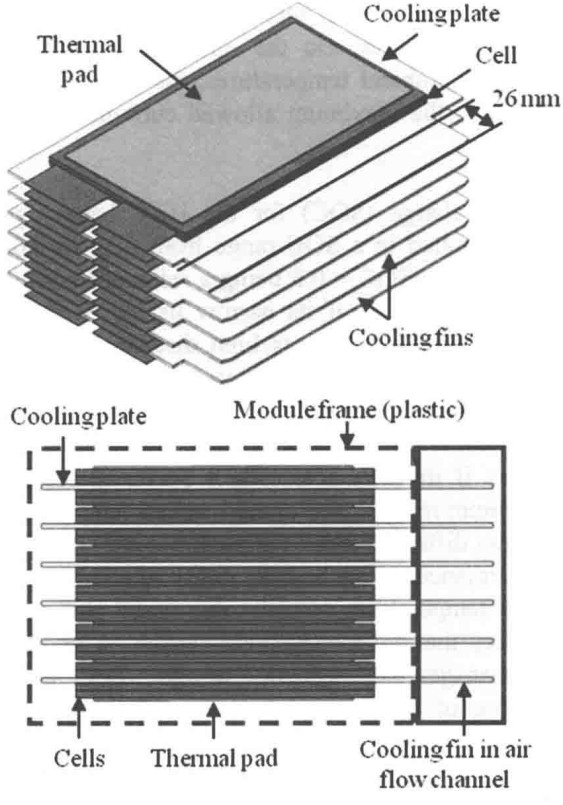

Figure 1. Battery module with indirect air cooling.

Table 1. Battery cell specification.

Cell Specifications	Lithium Manganese Oxide
Nominal capacity	8 Ah
Nominal voltage	3.75 V
Internal resistance	< 1.5mΩ
Operation temperatures	-25 to 60 °C
Mass	300 gram
Dimension (t × w × h) mm	6 × 128 × 240

BATTERY SYSTEM MODELING

As shown in the FEA model in Figure 1, the module has six cooling units. Figure 2 shows a representative cooling unit in the module. In modeling a battery cell in the cooling unit, the multi-layer structure of the battery cell [1,2] is simplified to a single equivalent battery layer which has a positive current collector and a negative current collector, a pair of electrodes (anode and cathode) and a separator. This single-layer battery cell is characterized with composite local thermal and electrical properties equivalent to those for the multiple-layered battery structure [3]. The composite local volumetric heat capacity are expressed as

$$\rho C_p = \frac{\sum_i \rho_i C_{p,i} V_i}{\sum_i V_i} \tag{1}$$

where the subscript i indicates the properties for the component i. The composite local thermal conductivities for the series and parallel connections are given respectively as

$$k = \frac{\sum_i L_i}{\sum_i (L_i / k_i)} \tag{2}$$

$$k = \frac{\sum_i L_i k_i}{\sum_i L_i} \tag{3}$$

In Eqs. (2) and (3), L_i and k_i are the thickness and the thermal conductivity for the component i respectively. Similarly, the composite local electrical conductivities can also be expressed by Eqs.(2) and (3) in characterizing the electrical field of the cell. In this study, the thermal behavior of the cells in the battery system under a given electrical load is characterized with energy balance on a unit cell volume as

$$\rho C_p \frac{\partial T}{\partial t} = \nabla \cdot (k \nabla T) + q \tag{4}$$

where ρ, C_p and k are the local density, heat capacity and thermal conductivity of the cell medium described in Eqs.(1), (2), (3), t is the time, T is the temperature and q is the rate of

local heat generation due largely to the cell ohmic heat resulting from the cell internal resistance and the cell discharge/charge currents [3].

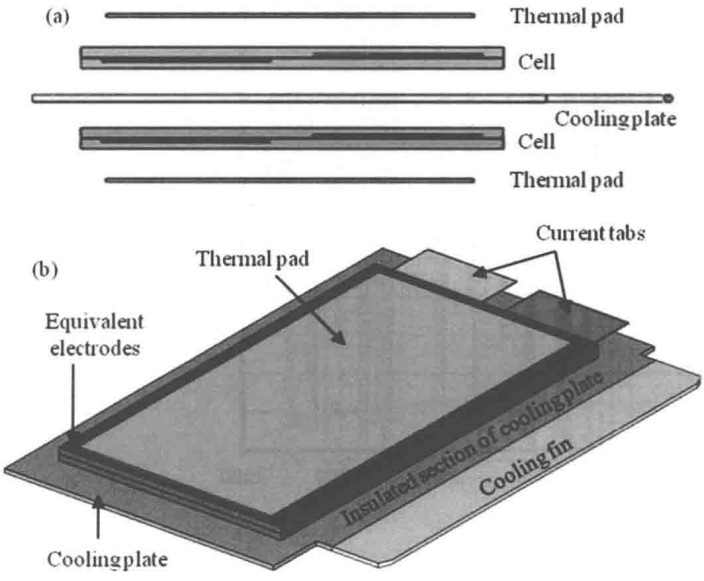

Figure 2. Basic cooling unit of the battery module: (a) exploded view; (b) assembled view with a single cell.

THERMAL ANALYSIS OF BATTERY SYSTEM

Battery Thermal Load Characterization

Figure 3 shows the simulated transient currents for the battery pack under a user specified cycle for a target hybrid vehicle. Because of the 96S1P pack configuration, the cell current is equal to the pack current. As shown in Figure 1, the components in the system lead to a large thermal inertia that mitigates the rises in the cell temperatures in the system. Like other electrical systems, a battery system can also tolerate electrical overloading in a short duration. In this study, the battery thermal load is evaluated on an $I^2\tau$ basis as

$$I_\tau = \sqrt{(\int_\tau i^2 dt)/\tau} \qquad (5)$$

where I_τ is a root-mean-square (rms) average current over a window time τ (i.e., the $I^2\tau$ current) and i is the transient current. Because τ is a moving window, $I_\tau = I_\tau(t)$ is a transient current in a thermal load sense, with the thermal history up to τ being considered [4]. The influence of the battery thermal history on the battery temperature depends on the levels of the disturbance to the battery internal energy by the heat generated by the dynamic current pulses. The shorter the window time, the smaller the effect of the thermal history on the battery temperature and the greater the dynamic behavior of the battery thermal loading will be. In this study, τ is taken to be 120 seconds considering the battery load level and the relatively high thermal mass in an indirect cooling system.

An equivalent continuous cycle current I_C can be defined as the average of the $I^2\tau$ current over the cycle time τ_C as

$$I_C = (\int_{\tau_C} I_\tau \times dt)/\tau_C \qquad (6)$$

The $I^2\tau$ current and the equivalent continuous cycle current or the averaged cycle current are also presented in Figure 3. The $I^2\tau$ current and the averaged cycle current are always positive, and their values are much lower than those of the transient current. The maximum values for the transient current i, the $I^2\tau$ current I_τ and the cycle average current I_C are, respectively, i_{max} = 200 A (equivalent to 25C rate), $I_{\tau,max}$ = 88 A (equivalent to 11C rate) and I_C = 48 A (equivalent to 6C rate). Since the cell heat generation is proportional to I^2, the $I^2\tau$ current characterizes the transient battery thermal load and the averaged cycle current characterizes the equivalent continuous battery thermal load.

Equivalent Continuous Load of the Battery System

There are two ways to characterize the thermal behavior of a battery system under the load condition specified in Figure 3: under the transient load characterized with the $I^2\tau$ current and under the equivalent continuous cycle current I_C [4]. As aforementioned, the equivalent continuous cycle load is 48 A or 6C rate. Because a battery cell is a finite energy system, the thermal equilibrium condition for the system cannot be reached under a single discharge process at 6C rate, for which a full discharge process lasts only 10 min. It is not practical to evaluate the thermal performance of a HEV battery system under a continuous current or power without controlling the SOC of the battery cells. Thus, a load profile with discharge and charge (i.e., regeneration) activities needs to be generated in order to constrain the SOC of the battery system in the range of the expected battery usage. Figure 4 shows a load profile considered in this study. In Figure 4(a), the current is given in values relative to the equivalent continuous current characterized with the 120-second window time, with the negative current for discharging and positive current for charging. The charge duration is about 90% of the discharge. The rest times are given as 5 seconds after discharging and 10 seconds after charging. Because the equivalent continuous current is on the $I^2\tau$ current basis, the same current is applied to both discharge and charge. The dynamic discharge-charge cycle of Figure 4(a) is repeated continuously resulting in cell load profile as shown in Figure 4(b). The corresponding SOC variations are also presented as a reference. The duration of the test is determined by the time required to reach thermal equilibrium.

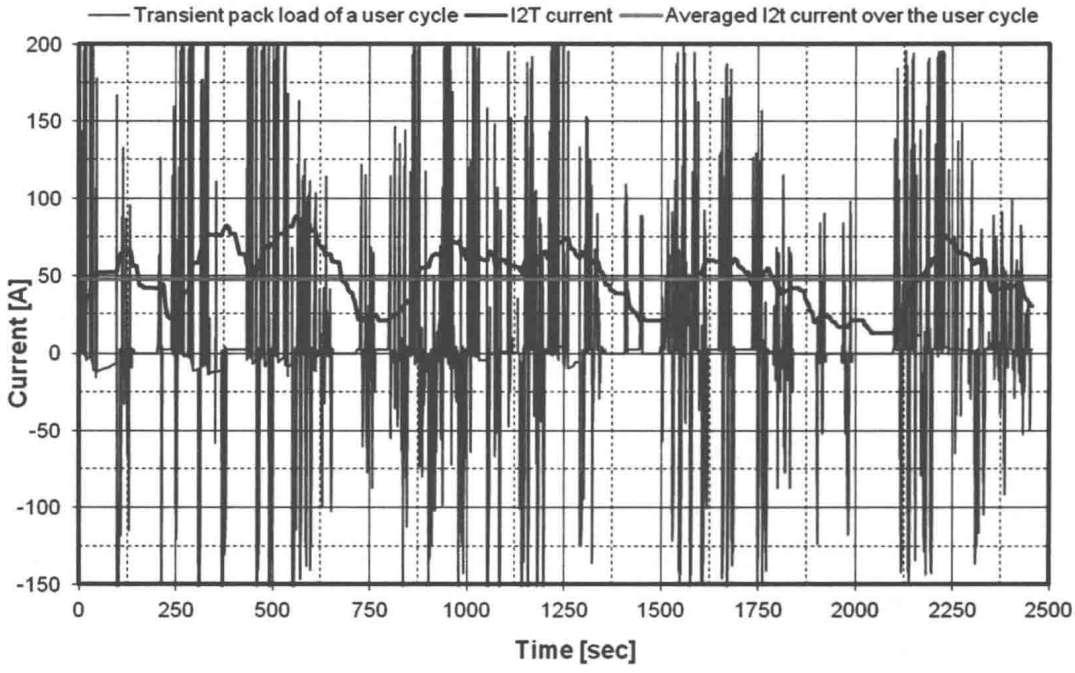

Figure 3. Transient pack load in a user cycle, $I^2\tau$ current and cycle averaged current for cell thermal evaluation.

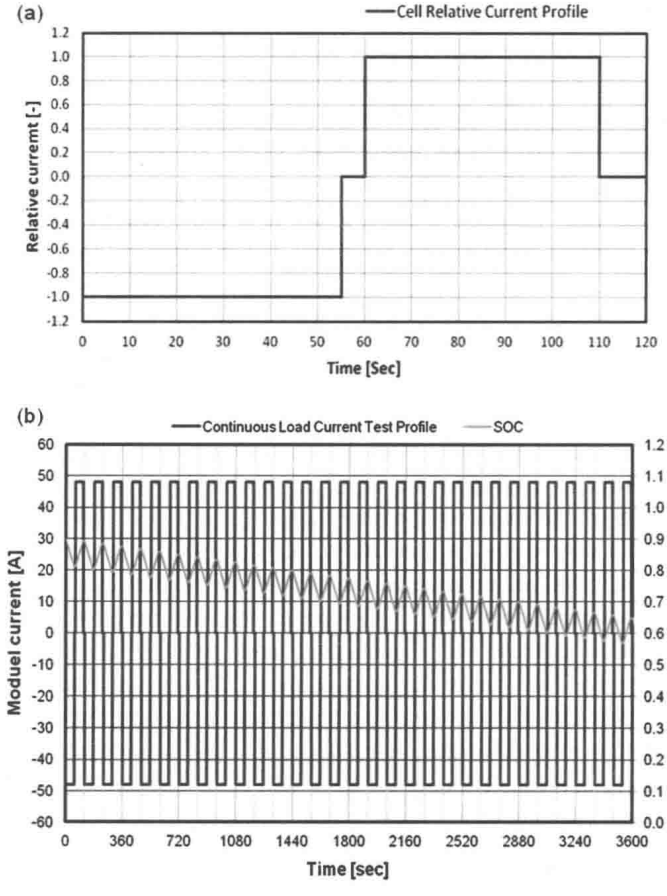

Figure 4. (a) Asymmetric relative current load profile for cell thermal evaluation; (b) Equivalent continuous current load using asymmetric load profile in (a) and the corresponding SOC variation.

Comparison of Simulation with Measurement

Figure 5 compares the simulated and measured cell and air temperatures under the load profile specified in Figure 4. A higher initial SOC value as shown in Figure 4(b) was used in the test because the run-time duration to reach thermal equilibrium was not known in advance. Based on the test conditions, the following initial and boundary conditions were used for the FEA model: the initial module temperature = 28.0 °C, the averaged air temperature = 26.5 °C, and the averaged HTC = 80 $W/m^2.K$ which correspond to module air flow ≈ 35 ft^3/min (CFM). It was assumed in the simulation that the cell heat is dissipated to the cooling air only through the cooling fins. Adiabatic conditions were assumed for the rest of the thermal boundaries of the module. Electro-thermal analysis of the battery module was performed using the FEA code Abaqus [5] with special user subroutines developed by AVL to characterize the cell. In Figure 5, the cell temperatures represent that of the cell in the middle of the module, which was least influenced by the variations in the ambient conditions. The red-dot indicates the location of the thermal couple on the cell in the test. As is observed in Figure 5, the simulations agree well with the measurements. Under the given cell load and cooling conditions, the battery module approaches thermal equilibrium after about 3600 seconds from the start of the test.

The simulated module temperature distribution at 3600 second is presented in Figure 6. It is seen that all the cells in the module have similar temperature distributions and the maximum cell temperatures are around 36 °C, located next to the adiabatic edge of the cooling plate, i.e., opposite side of

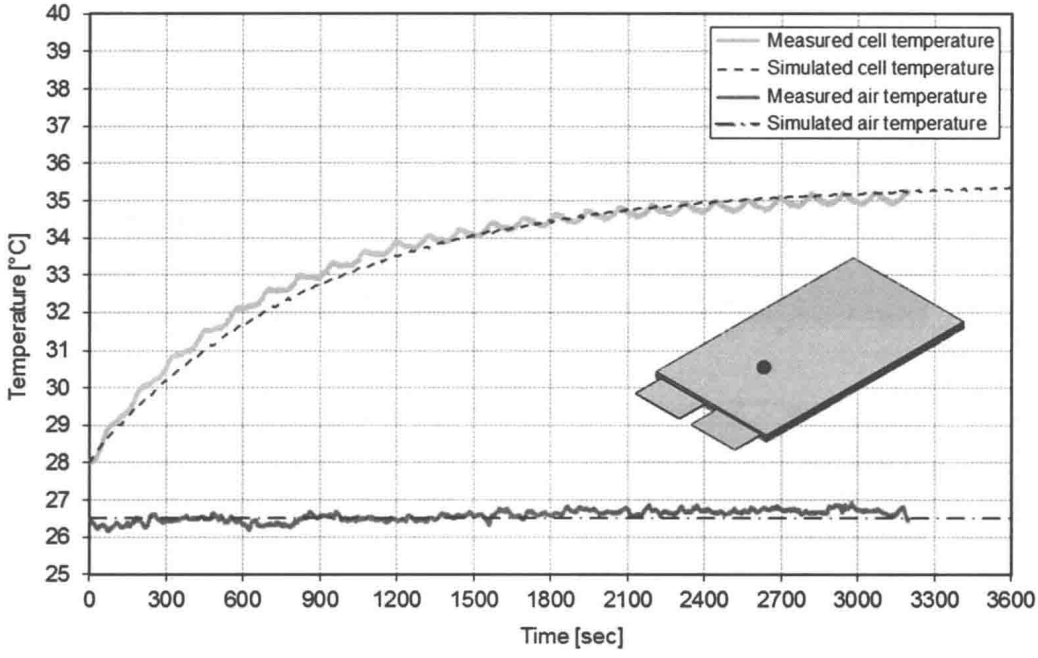

Figure 5. Transient cell temperatures under equivalent continuous discharge-charge load cycles.

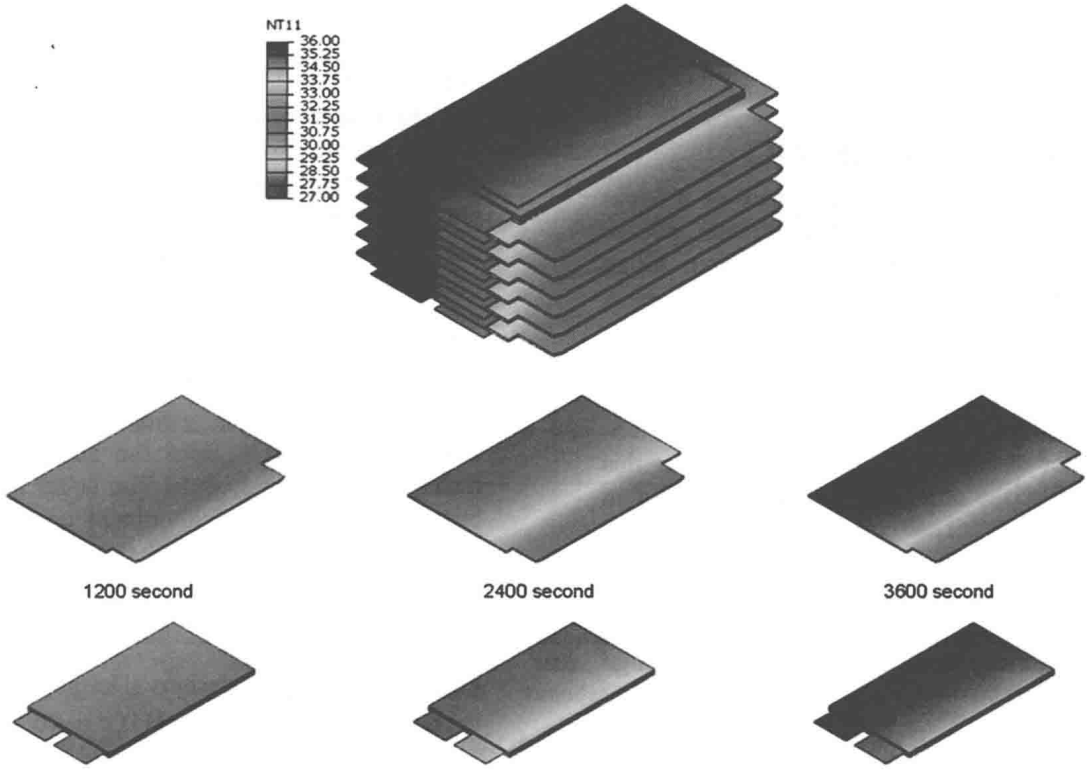

Figure 6. Module temperature distributions at thermal equilibrium (top); cell and cooling fin transient temperatures (bottom).

the cooling fin. The maximum cell-to-air differential temperature is about 11 °C. The low temperature gradients on the cooling fins suggest low fin efficiency, i.e., the cooling fin lengths in the air cooling channel are overdesigned [6]. Overdesign in the air cooling channel results in a lower volumetric energy density of the battery system. The temperature distributions for the cell and the corresponding cooling plate for the cooling unit in the middle of the module at 1200, 2400 and 3600 second from the start of the analysis are also presented in Figure 6. Since the two cells in the cooling unit are thermally symmetric, only the results for one cell in the cooling unit are presented. It is obvious that the cell temperature distribution is governed by the aluminum cooling plate due to its high thermal conductivity. The

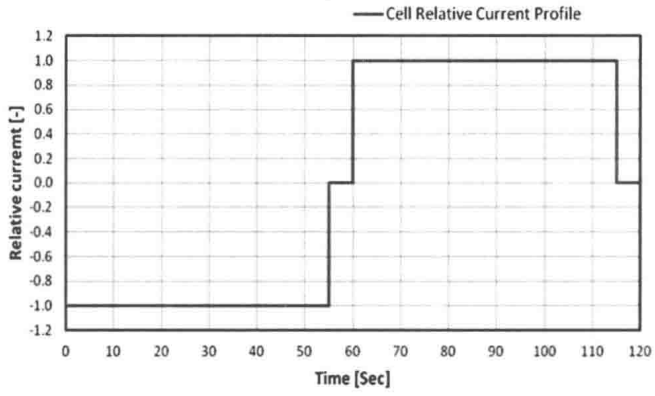

Figure 7. Symmetric discharge-charge analysis load profile.

temperature differences between the cell and the corresponding area of the cooling plate that is in contact with the cell are very small. This indicates that the cell temperature distribution is governed by the heat transfer characteristic of the cooling plate. This may be a characteristic of the indirect cell cooling: the cooling plate not only dissipates the cell heat to the cooling medium but it also functions as heat spreader which redistributes the high local cell heat fluxes.

IMPROVEMENT IN COOLING SYSTEM DESIGN

Load Profile with Balanced SOC

The cooling system described in Figure 1 leads to a lower volumetric energy density for the battery system due to overdesign in the air cooling channel. In this section, design improvement will be studied. Considering that a HEV pack generally is operated under a charge sustaining mode, for simplicity in analysis, the load profile is modified slightly. The modified load profile is shown in Figure 7, where the discharge and charge durations are 55 seconds each with a 5-second rest time after discharging and charging. Under this symmetric load profile, the charge sustaining is realized in each of the load profile. The corresponding equivalent continuous load profile is similar to that in Figure 4(b) except that the state of charge is balanced around SOC = 0.5 (the initial SOC value). In the analyses of the cooling system design study, the equivalent continuous discharge/charge currents are 48 A (6C rate).

Compact Air Cooling Channel Design

In an attempt to improve the energy density of the battery system, three alternatives are proposed as shown Figure 8. Design 1 is essentially the same as the baseline design except that the aluminum cooling plate thickness is changed from 2-mm to 1-mm. For Design 2, in addition to the 1-mm aluminum plate thickness reduction, the length of the cooling fins is reduced from 26 mm to 10 mm. Design 3 is the same as Design 2 but with air cooling channel structure similar to that of a compact heat exchanger - aluminum fin inserts (5 fins over 10 mm) are applied between the two cooling fins.

Figure 9 shows the simulated transient temperatures of the cell in the middle of the module for each of the four designs. The simulations were conducted at the initial module temperature = 25.0 °C, the averaged cooling air temperature = 25.0 °C, and HTC = 40, 50, 60 and 80 W/m^2.K for the alternative designs. For the baseline design, HTC = 60 W/m^2.K was used. As is seen in Figure 9, Design 2 (1-mm aluminum cooling plate and 10-mm wide cooling fins) does not reach thermal equilibrium at 3600 second for all three cooling conditions, and the cell temperatures are significantly higher than those of the baseline design. This alternative design is therefore unacceptable. For Design 1 (1-mm aluminum cooling plate and 26-mm wide cooling fins), only the case with HTC = 80 W/m^2.K is close to the performance of the baseline design. Overall, performances of Design 1 are not as good as those of the baseline design. Design 3 (1-mm aluminum cooling plate and 10-mm wide cooling fins with fin inserts) shows better performances than the baseline design for all cooling conditions. Hence this alternative design is acceptable from the standpoint of the thermal management of the module. The larger thermal mass for the baseline design (2-mm aluminum cooling plate) results in slower initial temperature rise in comparison to Design 1 and Design 3, both of which have a 1-mm thick aluminum cooling plate.

Figure 10 shows the designs (Design 1 with HTC = 80 W/m^2.K and Design 3 with HTC = 40 W/m^2.K) that have similar thermal performances as that of the baseline. It shows the stabilized cell temperatures plotted to the same scale at 3600 seconds from the start of the analysis. The temperatures and temperature gradients at the cooling fins for Design 3 indicate that it has higher fins efficiency.

Figure 11 shows the stabilized temperatures along the width of the cooling plate in the middle of the module. For the section of the cooling plate that is in contact with the cells, it also represents the temperature of the cells as the temperature

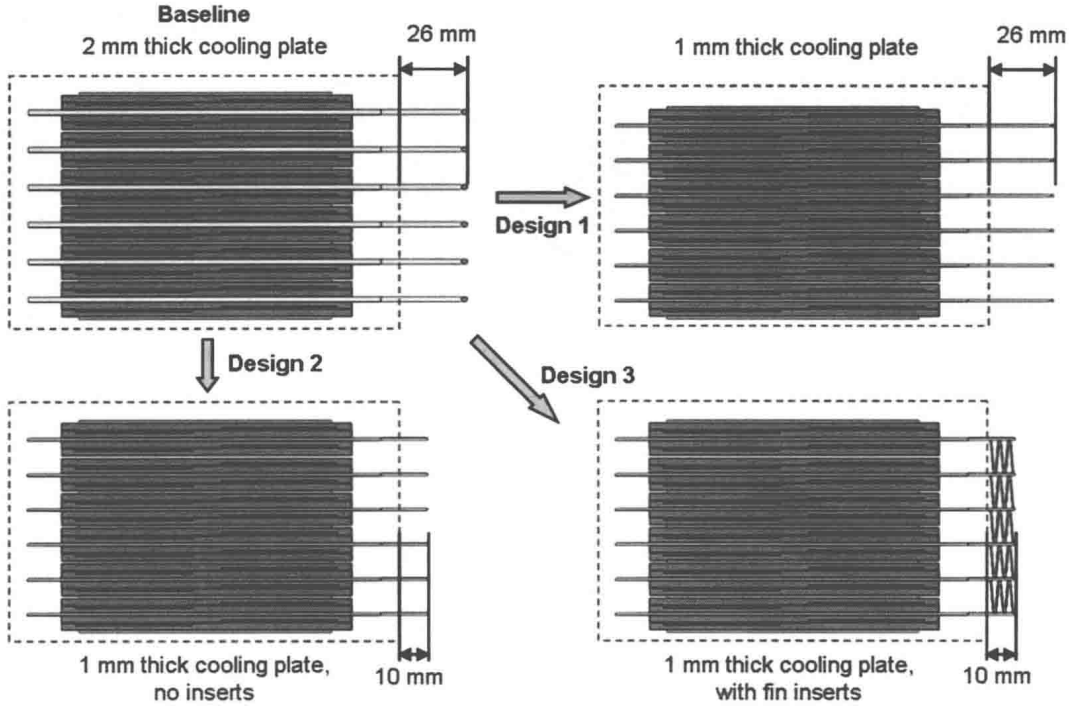

Figure 8. Baseline and alternative air cooling channel designs.

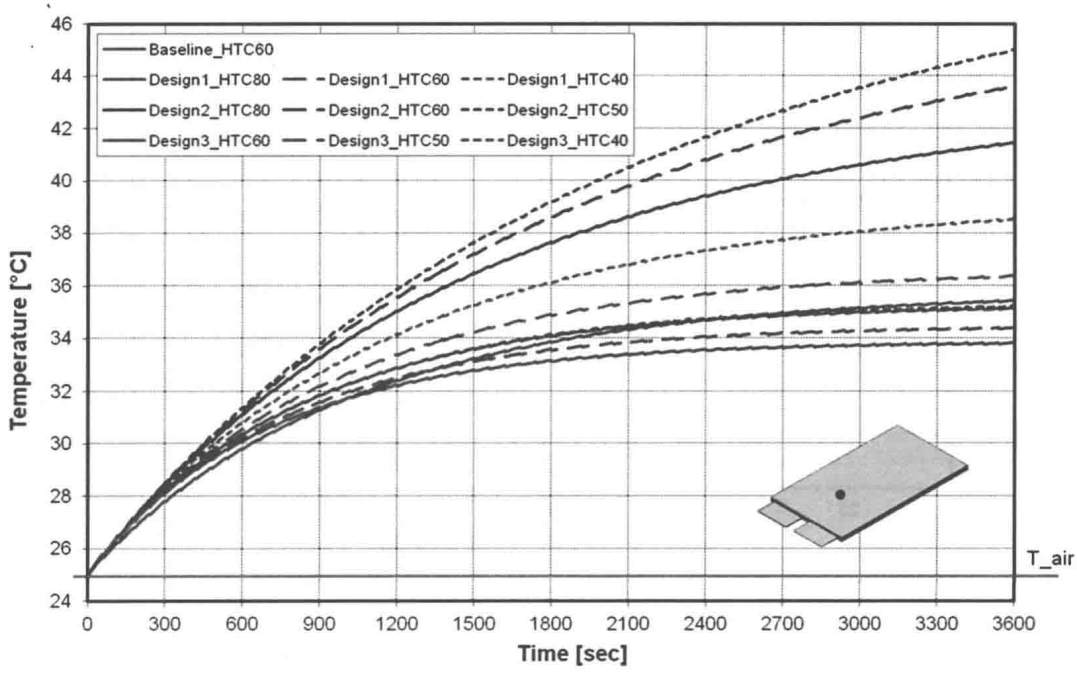

Figure 9. Transient cell temperatures for various module designs with different air flow rate under symmetric continuous discharge-charge load cycles.

differences between the cells and the corresponding area on the cooling plate in contact with the cells are negligible for all the cases analyzed. As before, the three designs presented have approximately the same stabilized cell temperatures. The baseline design with 2-mm thick aluminum cooling plate has lower thermal resistance compare to Design 1 and Design 3, which have a 1-mm thick aluminum cooling plate. This effect is clearly seen in the insulated section of the cooling plate. For the baseline design, the temperature drop along the cooling plate in the insulated section is 1.5 °C while the temperature drop of 3.0 °C is observed for Design 1 and Design 3. For Design 1, the change in cooling plate thickness reduces the module overall height by 6 mm as compare to the baseline. However, to achieve the same thermal performance as the baseline, higher HTC is needed at the cooling fins. Higher HTC means a higher air flow and thus a higher

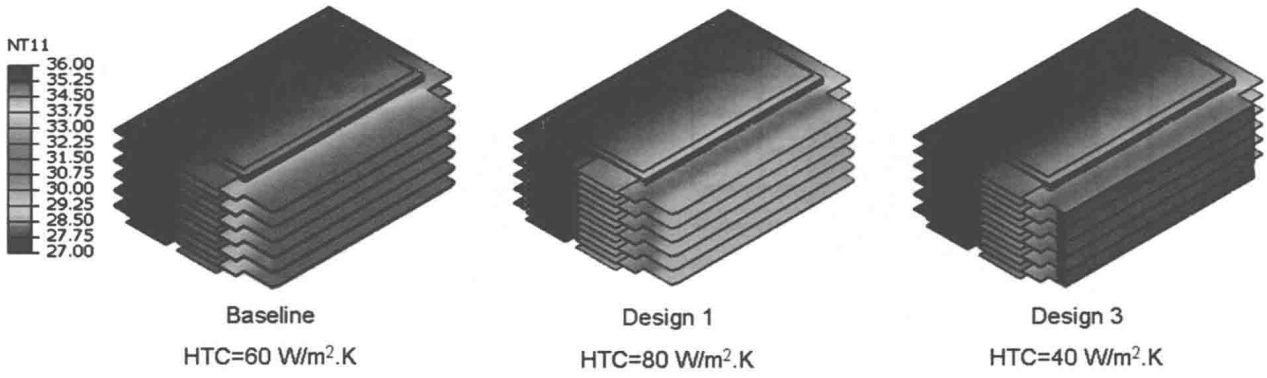

Figure 10. Stabilized cell temperatures for three module designs with approximately similar steady state temperature.

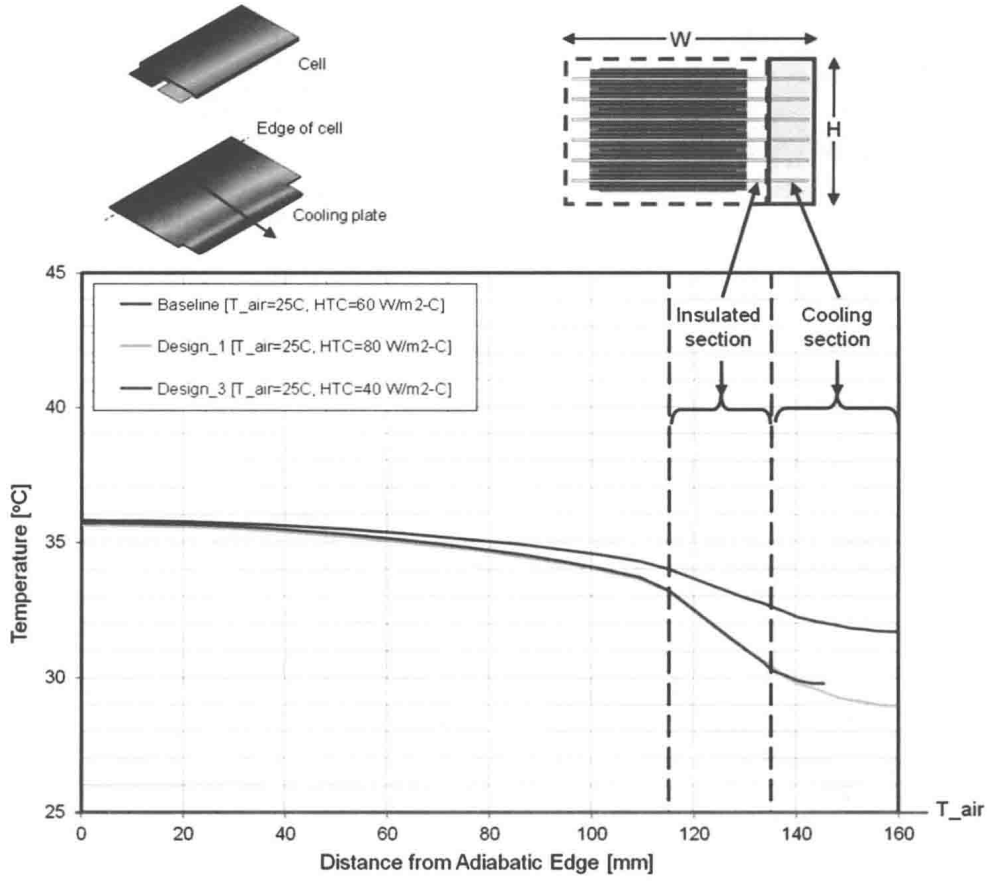

Figure 11. Steady state temperatures along the width of the cooling plate.

operation cost. Design 3 shows advantages in the thermal performance, energy density and operation cost. However, it has a higher initial cost due to the use of fin inserts in the air channels. Fin inserts are commonly use in compact heat exchangers thus their manufacturing cost may not be significantly higher than the straight fins.

SUMMARY

Thermal behavior of an 8Ah Li-ion battery system for HEV applications was investigated using FEA model for battery cooling. Thermal load for the battery system was due to the battery load specified in a user defined cycle for the target hybrid vehicle. The transient load for the cell thermal evaluation was generated by the $I^2\tau$ current with a 120-second window based on the transient currents in the cycle. The equivalent continuous cycle load was taken as the average of the $I^2\tau$ current over the cycle time. The cell temperatures were evaluated under the equivalent continuous cycle load until the battery module reaches thermal equilibrium. Analysis results correlated well with the available test data. Based on the correlated model, analyses were performed to evaluate alternative cooling system designs to improve the cooling performance and volumetric energy density of the